Rate and extent of protein localization is controlled by peptide-binding domain association kinetics and morphology

Evan Mills[1]* and Kevin Truong[1,2]

[1]Institute of Biomaterials and Biomedical Engineering, University of Toronto, Toronto, Ontario, Canada, M5S 3G9
[2]Edward S. Rogers Sr. Department of Electrical and Computer Engineering, University of Toronto, Toronto, Ontario, Canada, M5S 3G4

Received 18 February 2009; Revised 1 April 2009; Accepted 2 April 2009
DOI: 10.1002/pro.135
Published online 16 April 2009 proteinscience.org

Abstract: Protein localization is an important regulatory mechanism in many cell signaling pathways such as cytoskeletal organization and genetic regulation. The specific mechanism of protein localization determines the kinetics and morphological constraints of protein translocation, and thus affects the rate and extent of localization. To investigate the affect of localization kinetics and morphology on protein localization, we designed a protein localization system based on Ca^{2+}-calmodulin and Src homology 3 domain binding peptides that can translocate between specific localizations in response to a Ca^{2+} signal. We used a stochastic biomolecular simulator to predict that such a protein localization system will exhibit slower and less complete translocations when the association kinetics of a binding domain and peptide are reduced. As well, we predicted that increasing the diffusion resistance by manipulating the morphology of the system would similarly impair translocation speed and completeness. We then constructed a network of synthetic fusion proteins and showed that these predictions could be qualitatively confirmed *in vitro*. This work provides a basis for explaining the different characteristics (rate and extent) of protein transport and localization in cells as a consequence of the kinetics and morphology of the transport mechanism.

Keywords: synthetic biology; calmodulin signaling; SH3 binding domains; translocation; protein engineering

Introduction

Protein localization is a dynamic cellular process implicated in many aspects of cell function and control. Several examples of protein localization in a cellular context include targeting proteins to specific organelles after translation,[1] dynamic targeting of genetic transcription factors to the nucleus,[2] localization of enzymes, such as RhoA, during cytoskeletal reorganization,[3,4] or establishment of cell polarity, such as apical and basal membranes in endothelial cells.[5] Protein localization targeting can be controlled constitutively or dynamically. For example, proteins expressing a C-terminal Lys-Asp-Glu-Leu (KDEL) peptide will be constitutively retained in the endoplasmic reticulum.[6] Dynamic control over protein localization can be regulated by the selective presentation of nuclear localization or export signals (NLS and NES, respectively), as is the case in p53,[7] Kir/Gem GTPases,[8] and the sex-determining protein Sry,[9] or by control of upstream signals, such as pro-survival kinases which phosphorylate the pro-apoptotic protein Bad and sequester it in the cytoplasm.[10]

Grant sponsor: Canadian Foundation of Innovation; Grant number: 10296; Grant sponsor: Canadian Institutes of Health Research; Grant number: 81262; Grant sponsor: Heart and Stroke Foundation; Grant number: NA6241; Grant sponsor: Natural Science and Engineering Research Council; Grant number: 283170.

*Correspondence to: Evan Mills, Institute of Biomaterials and Biomedical Engineering, University of Toronto, 164 College Street, Toronto, Ontario, Canada, M5S 3G9. E-mail: e.mills@utoronto.ca

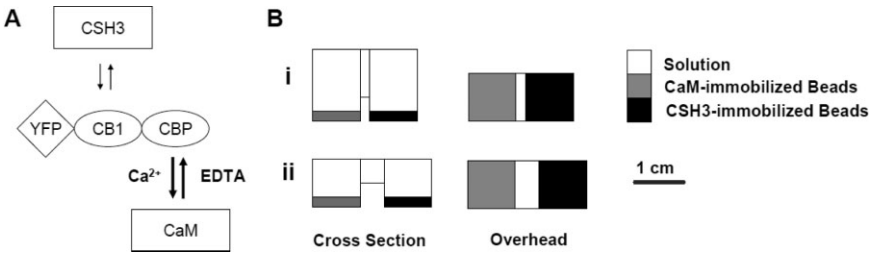

Figure 1. Schematic diagram of the protein localization system. A, The sensor protein and its selective interaction with CaM-immobilized beads given a Ca^{2+} signal and constitutive interaction with CSH3-immobilized beads. B, Two wells, each with a separate population of beads, are separated by a connecting bridge. i is termed the compact well structure because the wells are closer to each other than in ii, the extended well structure.

The characteristics of protein localization (rate and extent of localization) can be affected by intrinsic properties of the protein as well as the environment. The localization kinetics will determine how rapidly a protein will respond to a localization signal. For example, caspase-mediated cell death is a relatively fast-acting pathway, and so pro-apoptotic protein localization to the mitochondria must be achieved quickly.[11] This is in contrast to changes in genetic regulation which occur over many hours to days, and so localization of NLS-expressing transcription factors to the nucleus need not be as rapid.[12,13] Another variable to influence protein localization is the morphology of the environment. The morphology of different cellular environments can vary widely, from long and narrow processes of neuronal axons, extended and flattened morphology of epithelial and fibroblast cells,[14] or the distinctive biconcave shape of erythrocytes.[15] The effect that morphology may have on cellular processes is often noted in the context of a comparison between biological systems and electrical circuits.[16]

To investigate the dynamic properties of protein localization, we simulated and implemented a protein localization system of synthetic proteins that can translocate between specific localizations in response to a Ca^{2+} signal, inspired by naturally occurring calmodulin-mediated protein translocations.[8,9] This protein localization system uses three protein domains and interactions: calmodulin (CaM) and CaM-binding peptides (CBPs), yellow fluorescent protein (YFP), and the N-terminal Src homology 3 (SH3) domain of human Crk2 (CSH3) and its binding peptide, CB1. CaM is a ubiquitous family of proteins that bind target peptides in the presence of Ca^{2+}.[17] Two different CBPs have been used because they bind Ca^{2+}-CaM with different affinities: the CBP of CaM kinase kinase (CKKp) which has high affinity for Ca^{2+}-CaM (dissociation constant, K_D: 4.0 ± 0.5 n*M*),[18] and the CBP of CaM kinase 4 (CaMK4p) which has a moderate affinity for Ca^{2+}-CaM (K_D: 158 ± 42 n*M*).[19] YFP will be used as a sensor because it has been used as a reporter of protein localization previously.[20] Finally, the constitutive binding of CSH3 to CB1, a peptide cloned from the guanine nucleotide exchange factor C3G, will also be used because of its relatively weak affinity (K_D: 1.89 ± 0.06 μ*M*).[21]

Stochastic simulations of this protein localization system allowed us to predict the effects of kinetics and morphology on the system's behavior. We chose stochastic simulations because this method is better suited to considering the effects of localization such as molecular crowding[22] which may occur in areas of high molecular traffic, or noise effects due to low concentrations.[23–26] As well, a stochastic implementation will allow for translocation through complex geometries to be considered, which could only be handled with computationally expensive partial differential equations deterministically. The simulation predictions were then compared with the experimental results from the implementation of this localization system using synthetic fusion proteins.

Results and Discussion

Conceptual design of a protein localization system

Conceptually, a simple protein localization system can consist of a protein sensor that translocates from one location to another when Ca^{2+} is high and returns to the original location when Ca^{2+} is low (see Fig. 1). This design was inspired by naturally occurring proteins such as Kir/Gem and Sry which use CaM to convert a Ca^{2+} signal into a specific subcellular localization.[8,9] Such a protein sensor can be created from the tandem fusion of YFP, CB1, and CBP (hereafter, named YFP-CB1-CBP). When Ca^{2+} is low, the sensor associates with a CSH3 domain by its CB1 peptide whereas when Ca^{2+} is high, the sensor associates strongly with CaM by its CBP peptide. Since the Ca^{2+} can be added to the solution and removed by a Ca^{2+} chelator such as EDTA, the localization of the YFP-CB1-CBP sensor could be changed by selectively encouraging the association of CB1 with CSH3 or CBP with CaM [Fig. 1(A)]. To define two separate locations for the YFP-CB1-CBP sensor to translocate between, CSH3 and CaM domains can be immobilized by sepharose beads into two wells connected by a bridge that allows for the sensor to diffuse between the wells

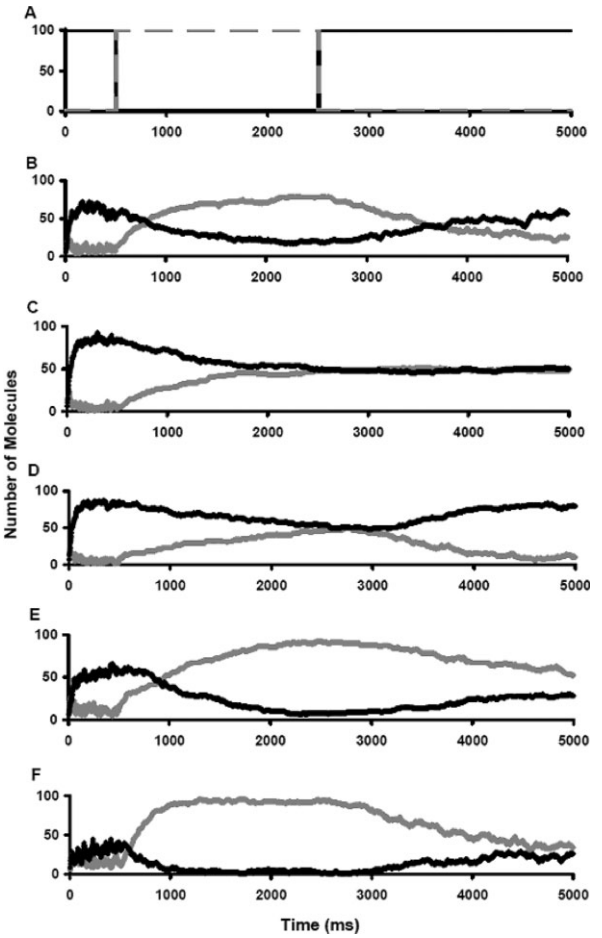

Figure 2. Effect of binding kinetics on localization system behavior. The number of sensor molecules bound to CSH3-immobilized beads is shown in black; the number of sensors bound to CaM-immobilized beads is shown in gray. The inputs are the same as in the ideal simulation. Each panel represents a different set of kinetics parameters, which will be stated as an ordered pair (CaM-CBP K_D, CSH3-CB1 K_D), values in M. Panel A (Ideal response), Panel B (10^{-7}, 10^{-6}), Panel C (10^{-9}, 10^{-7}), Panel D (10^{-7}, 10^{-7}), Panel E (10^{-8}, 10^{-6}), and Panel F (10^{-7}, 10^{-5}).

[Fig. 1(B)]. Given that the sensor is tagged with YFP, the localization of YFP-CB1-CBP can be observed by comparing the fluorescence signal between each well.

Although the size and shape of our *in vitro* model is not strictly analogous to intracellular physiological conditions, the model is still useful because it can describe relative changes in the parameters that we are studying, namely, association kinetics and morphological dimensions. The model allows translocation because proteins are "pulled" in one direction as the system attempts to re-establish equilibrium. This is similar to several examples of cellular translocation such as dynamic translocation of protein kinase C (PKC) between the membrane and the cytoplasm. The affinity of PKC for membrane structures is regulated by phosphorylation and Ca^{2+}.[27] In our model, we have used peptides with different affinities for localization structures as a representation of the dynamic changes possible in endogenous proteins. As such, each peptide in our model could be considered to represent a different functional state of a particular protein, and be tailored to a given protein of interest. In terms of morphology, several translocation conduits are known to dynamically change size and shape, such as the NPC which dilates and contracts in response to large cargos[28] and ATP[29] or Ca^{2+},[30] respectively. Our model reflects these different situations by allowing for different morphological arrangements to be considered.

Simulated effect of peptide-binding domain kinetics on the localization system

Stochastic simulations of the simple system described earlier show that it can translocate between two specific localizations, but large differences between the relative binding kinetics of CB1-CSH3 compared to CBP-CaM can abrogate the ability to translocate altogether, while minor kinetics differences can augment translocation speed, fluctuations, and completeness of translocation (see Fig. 2). Using our stochastic simulator based on previous designs,[22,24,25,31–38] the localization system was first simulated with kinetics parameters similar to the CB1-CSH3 (1.89 ± 0.06 μM)[21] and Ca^{2+}-loaded CKKp-CaM (4.0 ± 0.5 nM)[18] associations reported in the literature. The Ca^{2+}-loaded CKKp-CaM association was chosen to be stronger than the CB1-SH3 association because in the presence of Ca^{2+}, CKKp-CaM association was expected to drive the localization to the CaM-immobilized beads. In the absence of Ca^{2+}, the CKKp-CaM association is negligible. The removal of Ca^{2+} was mediated by addition of excess EDTA (~1 nM).[39] To increase the speed of the simulation, the dimensions of the two-well structure above were a scaled down from cm to μm. The specific reactions and reaction parameters are summarized in Table I.

Table I. *Simulation Reactions and Parameters*

Forward reaction	K_D (M)	k_{on} (M^{-1} s^{-1})	Reference
Ca^{2+}+EDTA→CaEDTA	10^{-9}	10^{10}	35
Ca^{2+}+apoCaM→Ca^{2+}−CaM	10^{-6}	10^{7}	17–19
Sensor+Ca^{2+}−CaM→Ca^{2+}−CaM−Sensor	10^{-8}–10^{-6}	10^{9}–10^{7}	18,19
Sensor+CSH3→CSH3−Sensor	10^{-5}–10^{-5}	10^{8}–10^{6}	21

For brevity, the fusion protein Ven-CB1-CBP has been called "Sensor" in Table I. The reverse reaction rate, k_{off}, can be calculated from the given data.

Our standard simulation consisted of three phases: an initial diffusion phase, a Ca^{2+}-translocation phase and an EDTA-translocation phase [Fig. 2(A)]. During the diffusion phase, 100 sensor molecules were added to the bridge region (so as not to bias the initial localization) and allowed to diffuse for 500 ms. Because of the constitutive association of CB1 to CSH3, the sensor should localize to the CSH3-immobilized beads. Second, during the Ca^{2+}-translocation phase, a Ca^{2+} signal was added at 500 ms. The stronger association between CaM and its CBP compared to that of CB1 and CSH3 should cause localization to the CaM-immobilized beads. Finally, during the EDTA-translocation phase, the Ca^{2+} signal was removed at 2500 ms by adding excess EDTA and the simulation was allowed to run until 5000 ms. During this phase, the constitutive association between CB1 and CSH3 should dominate again. Ideally, a translocation signal should result in instantaneous changes in localization with no fluctuation of localization between signals [Fig. 2(A)].

When this system was simulated, non-ideal behavior was manifested in three ways: a non-instantaneous response from input signal to localization, fluctuations in the localization between signals, and incomplete localization of sensor molecules to the predicted region [Fig. 2(B)]. The slow response time from input to output was the result of physical realities such as the time required for sensor molecules to diffuse from the bridge to a well and the time required for molecular collisions to result in peptides associating with binding domains. Fluctuations in localization were due to diffusion and random dissociations occurring at the same time as association. A consequence of this was that the localization of sensor molecules was never complete and some sensors were found in the bridge region or in the opposing well region.

Next, we investigated the effect of the peptide-binding domain association kinetics on the behavior of the localization system [Fig. 2(C–F)]. In these simulations, all parameters were held constant except for the association kinetics between CB1 and CSH3 or CBP and CaM. In simulations where the CB1-CSH3 association was very strong compared to the CBP-CaM association, the sensor could not translocate from the CSH3-immobilized beads to the CaM-immobilized beads during the Ca^{2+}-translocation phase [Fig. 2(C,D)], while if the CBP-CaM association was too strong, the sensor's return to the CSH3-immobilized beads was impaired during the EDTA-translocation phase [Fig. 2(E,F)]. These simulations suggest that the association kinetics between a translocating protein and its binding domains are crucial in ensuring that some molecule can translocate effectively between two locations. Specifically, a protein localization system whose association kinetics corresponds to CB1-CSH3 and CKKp-CaM can translocate between two locations in response to a Ca^{2+} signal [Fig. 2(B)].

Simulated effect of the morphology of the well structure on the localization system

Stochastic simulations of the localization system with the compact and extended well structures show that when the bridge pathway connecting the wells has a reduced cross-sectional area and is elongated, the translocation is slower and less complete than for a shorter, higher cross-sectional area diffusion path. To investigate the effect of the morphology of the well structure on the localization system, our standard simulation described above was performed using the CB1-CSH3 and CKKp-CaM association kinetics in the compact and extended well structures. The extended well structure exhibited longer translocation time constants [the time required to achieve $(1-e^{-1})$ of the final value] during both the diffusion phase and Ca^{2+}-translocation phase. The extended well structure exhibited longer translocation time constants [the time required to achieve $(1-e^{-1})$ of the final value] during both the diffusion phase (32 ± 1 ms for extended vs. 25 ± 1 ms for compact) and Ca^{2+}-traslocation phase (430 ± 5 ms vs. 400 ± 5 ms). Also, interestingly, the extended well structure suffered from a less complete localization, as seen by the lower steady state localization compared to the compact well structure ($50 \pm 2\%$ for extended vs. $65 \pm 3\%$ for compact in the diffusion phase, and $85 \pm 3\%$ vs. $92 \pm 2\%$ in the Ca^{2+}-translocation phase). The reduction in output signal was due to the increased volume of the bridge region, which contains unlocalized sensors, as well as the reduced likelihood that sensors will diffuse across the bridge with a smaller cross-sectional area.

In vitro *characterization of the peptide-binding domain associations of the protein sensors*

To implement the protein localization system *in vitro*, we created two protein sensor variants: First, Ven-CB1-CKKp—the tandem fusion of Venus (YFP variant),[20] CB1 (peptide has a weak association for CSH3, K_D 1.89 ± 0.06 μM),[21] and CKKp (peptide has a strong association with Ca^{2+}-CaM, K_D 4.0 ± 0.5 nM)[18]; second, Ven-CB1-CaMK4p—the tandem fusion of Venus, CB1, and CaMK4p (peptide has a moderate association with Ca^{2+}-CaM, K_D 158 ± 42 nM).[19] To immobilize the CSH3 domain to glutathione-sepharose beads, we also created the fusion protein CSH3-mRFP-GST—the tandem fusion of CSH3,[21] mRFP,[40] and GST. We verified the association interactions and our measurement techniques with the reversible binding of Ven-CB1-CKKp to CaM-immobilized beads, and then we examined the binding of Ven-CKKp to CaM beads in our well structures. Throughout, we used relative brightness of images to quantify association as a "localization ratio."

Ven-CB1-CKKp showed Ca^{2+}-dependent reversible association of the sensor with CaM-immobilized beads (see Fig. 3). The images show strong localization of the sensor to the CaM beads sequestered at the tip of

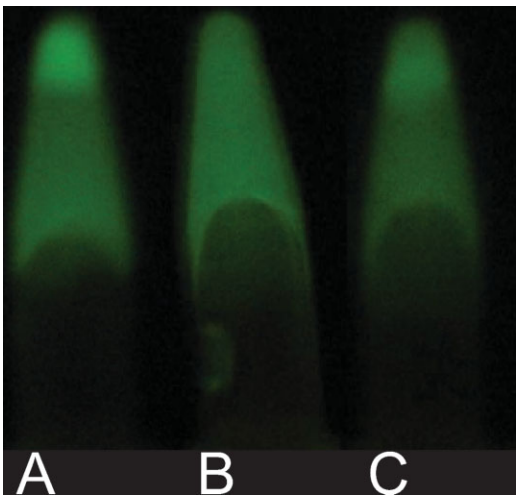

Figure 3. CaM beads assay with Ven-CB1-CKKp construct. CaM-immobilized beads were sequestered at the tip of a 1.5 mL tube (top). The solution was 1 mL of ~10 μM protein construct. The pictures represent three time points under different conditions: 1 mM $CaCl_2$ (Panel A), 2 mM EDTA (Panel B), and 4 mM $CaCl_2$ (Panel C). [Color figure can be viewed in the online issue, which is available at www.interscience.wiley.com.]

a 1.5 mL tube in a 1 mM Ca^{2+} solution [Fig. 3(A)]. Binding is not observed when EDTA is added [Fig. 3(B)] and returns partially when Ca^{2+} is re-introduced [Fig. 3(C)]. The corresponding localization ratios are shown (Table II) where a ratio greater than one corresponds to sensor localization in the tip of the tube and a ratio of one corresponds to no preferential association. A similar experiment was conducted between Ven-CB1-CKKp and CSH3-immobilized beads using positive and negative controls to confirm the constitutive association (data not shown).

To verify that a sensor associating with beads in the two-well structures could produce a fluorescence distribution that could be quantified with a localization ratio, we tested Ven-CKKp in the two-well structure because this construct should produce strong association with CaM-immobilized beads and very little association with CSH3-immobilized beads. Images were captured from the cross-section and overhead views [Fig. 4(A,B), respectively). The cross-section view shows strong sensor association to the CaM-immobilized beads, however, this is less obvious by inspection in the overhead image due to background light and a more diffuse fluorescence signal in that plane. However, the localization ratio for this image (CSH3 well/CaM well) is 0.61 ± 0.04, which indicates significant association between Ven-CKKp and CaM beads.

This experiment also provides validation for the use of a stochastic algorithm. The fluorescence distribution in the bead layer of the left well [Fig. 4(A)] clearly shows that the beads and Ven-CKKp solution is non-homogeneous. This was expected since Ven-CKKp is limited in movement by diffusion, thus it cannot penetrate below the surface of the beads. Such a distribution is well suited to a stochastic model rather than a deterministic one.[22,24,25]

Protein sensors translocate in response to a Ca^{2+} signal

The implementation of the protein localization system showed that the protein sensors could translocate in response to a Ca^{2+} concentration signal (see Fig. 5). An experiment was created to mimic our standard simulation as closely as possible. Concentrations and arrangements of molecules were consistent with the simulations, using the compact well structure. The sensor (Ven-CB1-CKKp) was given 24 h to achieve its steady state localization after each input signal. In the ratio analyses, background light has been accounted for, as well as leak-through of mRFP into the 520 nm filter.

The signal is faint to the naked eye (see Fig. 5), however, careful inspection of the diffusion phase image [Fig. 5(B)] showed increased fluorescence signal from the CSH3 well (right side of image), and then increased fluorescence in the CaM well (left side) during the Ca^{2+}-translocation phase [Fig. 5(C)]. The higher fluorescence signal in the CSH3 well during the diffusion phase is due to the constitutive association between the sensor's CB1 peptide and the CSH3-immobilized beads in that well. The higher fluorescence signal in the CaM well during the Ca^{2+}-translocation phase is due to the Ca^{2+}-dependent association between the sensor's CKKp peptide and CaM-immobilized beads in that well. The difference between signals in the EDTA-translocation phase [Fig. 5(D)] is marginal, which is consistent with simulation predictions [Fig. 2(B)].

This experiment has shown that the bulk of a population of fusion protein sensors can translocate reversibly in response to a Ca^{2+} signal, which is consistent with our simulations. The extent of the localization in the experiment [Fig. 5(B)] is not as complete as the

Table II. *Analysis for the CaM/Ven-CB1-CKKp Binding Assay*

Measurement	Figure 3A (1 mM Ca^{2+})	Figure 3B (2 mM EDTA)	Figure 3C (4 mM Ca^{2+})
Beads brightness*	97.3 ± 1.5	68.3 ± 2.1	68.0 ± 3.0
Solution brightness*	60.0 ± 1.0	69.0 ± 2.0	52.7 ± 1.5
Localization ratio	1.62 ± 0.04	0.99 ± 0.04	1.29 ± 0.07
Observed association	Strong	None	Partial

Results are shown as mean ± standard deviation, $n = 3$.
* Brightness measurements range from 0 to 256 where 0 is black.

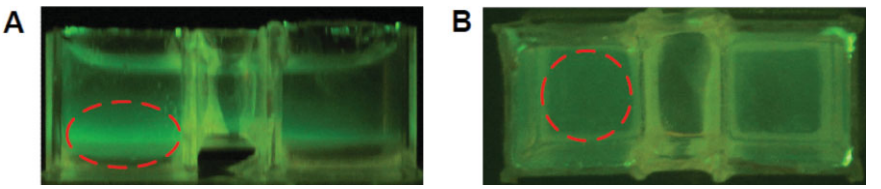

Figure 4. Profile and overhead view of the CaM-associating sensor Ven-CKKp. The CaM well is always presented as the left well in a figure and the CSH3 well as the right well. A, Profile view with fluorescence localized to CaM-immobilized beads shown in red oval. B, Overhead view with fluorescence localization to CaM-immobilized beads shown in red circle.

simulations predicted [Fig. 2(B)]. This is likely due to several factors including non-ideal mixing of the solution, association kinetics that may have been perturbed due to the presence of Ven or mRFP and non-linearity between the fluorescence signal and the resultant brightness analysis. However, given that the localization ratio trend increased above 1 and decreased below 1 in the expected phases (diffusion and Ca^{2+}-translocation phases, respectively), the bulk of the sensor population has translocated as expected in response to the Ca^{2+} signals.

Experimental effect of CaM-CBP kinetics on the localization system

Augmenting the Ven-CB1-CKKp sensor with CBPs with weaker CaM-association kinetics increases the time constant of the sensor translocation and causes slower localization of sensors to the desired state [Fig. 6(A)]. We studied localization kinetics by designing two sensor variants with two peptides each with different affinities for the localization mechanism: association to CaM-immobilized beads. To determine the extent of kinetics' effects *in vitro* a time course experiment was performed using the Ven-CB1-CKKp and Ven-CB1-CaMK4p sensors.

We predicted that the first translocation during the diffusion phase should be similar for both constructs because the CB1-CSH3 kinetics have not been directly altered. However, the Ca^{2+}-translocation phase should be much slower for the sensor with a CaMK4p CBP than the sensor with the CKKp CBP. To investigate this effect, the experiment in the compact well structure, above, was repeated with both sensor variants in two different well structures simultaneously. Images of both experiments were captured in the same photograph at indicated intervals after the signal was introduced [Fig. 6(A)].

The localization ratio time course shows two general trends. First, the diffusion phase translocation is not affected when the CBP is changed, which was expected since the CSH3 binding peptide has not been affected directly or indirectly by steric hindrance. The second trend is that the Ca^{2+}-translocation phase translocation from the CSH3 localization to the CaM localization is significantly delayed, and the steady

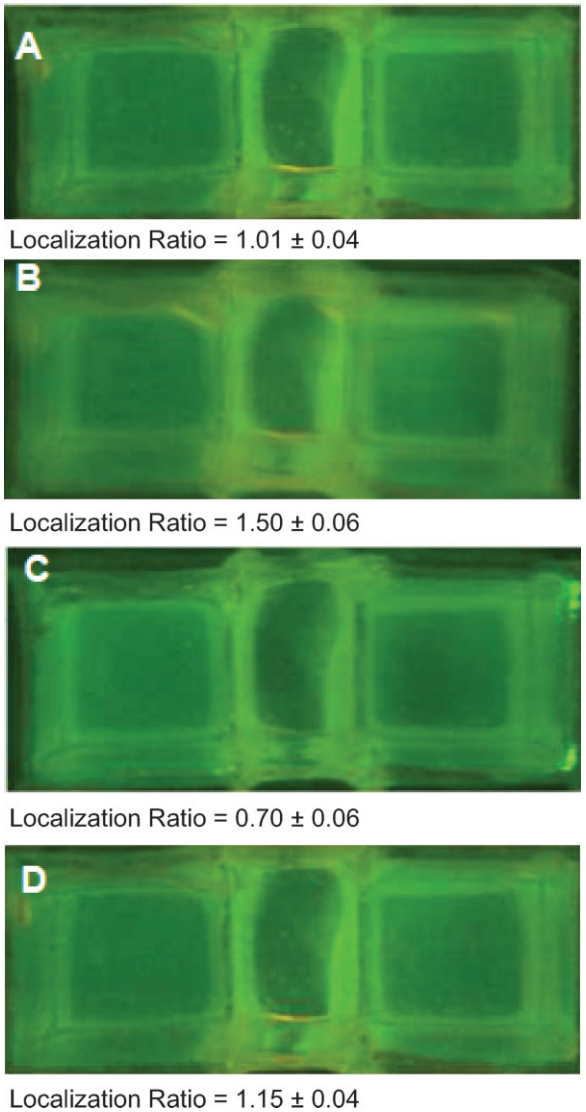

Figure 5. Experiment showing alternating localization of the localization system. Again, the CaM well is the left well and CSH3 well is the right well. The same experiment from the simulations was repeated here: Images were taken immediately after sensor added at $t = 0$ h (Panel A), after 24 h in buffer with 1 m*M* EDTA (diffusion phase, Panel B), after 24 h (48 h total) in a buffer with 1 m*M* EDTA +2 m*M* $CaCl_2$ (Ca^{2+}-translocation phase, Panel C), and 24 h (72 h total) in a buffer with 2 m*M* $CaCl_2$ + 4 m*M* EDTA (EDTA-translocation phase, Panel D). Localization ratios are state under each image as mean ± standard deviation, $n = 3$.

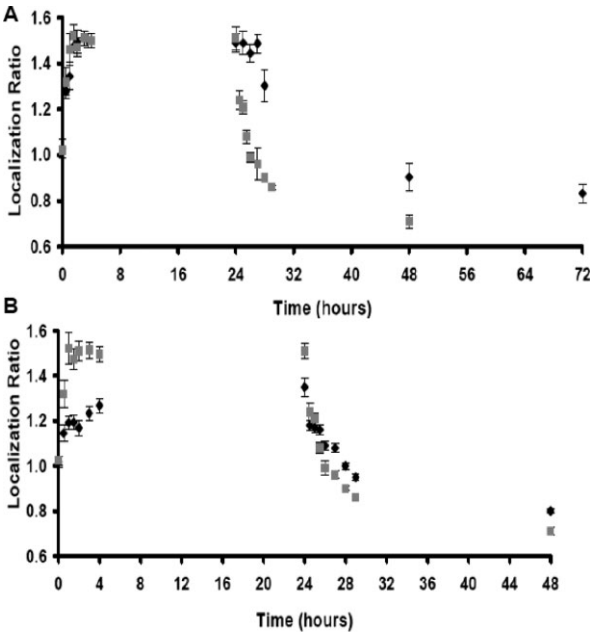

Figure 6. Comparison of translocation behavior for (A) CBP sensor variants and (B) well structure variants. The localization ratio is presented over time for the two variant conditions during the diffusion phase translocation (0–24 h) and then the Ca^{2+}-phase translocation. The first signal, at 0 h, brings the solution to 1 m*M* EDTA, and the second signal, at 24 h, brings the solution to 2 m*M* $CaCl_2$. Legend: Panel A, Black diamonds CaMK4p variant, gray squares CKKp variant; Panel B, Black diamonds extended well structure, gray squares compact structure. Error bars are standard deviation, $n = 3$.

state localization ratio is also reduced. Both of these predictions coincide with our simulations where the CaM-association kinetics has been reduced from a low n*M* order interaction, as with CKKp, to a high n*M* interaction, as with CaMK4p. These results show that we were able to qualitatively predict the effect of kinetics on the localization system.

Different protein localization events occur at different rates, and the rate of localization could be linked to the association kinetics between a localization peptide on a protein and some cellular localization mechanism. For example, NLS and NES signals have a relative "strength," suggesting stronger signals interact with importins and exportins with higher affinity than weaker signals.[2,41] This difference in localization kinetics is important in determining the relative distribution of some proteins that express both NLS and NES peptides, such as p53.[7] By changing the association kinetics of our sensor's CBP, we have demonstrated that changes in protein localization rate and completeness are consequences of the affinity of a protein for its localization mechanism.

Experimental effect of the morphology of the well structure on the localization system

The extended well structure has reduced the steady state localization ratio of the protein localization system and has increased the time constant of the diffusion phase translocation in comparison to the compact well structure [Fig. 6(B)]. We modified the *in vitro* experiment to use the same sensor (Ven-CB1-CKKp) in the compact and extended well structures. As with the previous experiment, images of both apparatuses were taken in the same photograph. The extended well structure localization ratio showed that sensor translocations occurred with larger time constants and less complete localization than the compact well structure. Both of these trends were predicted from simulations.

The morphology in which proteins must localize can vary between cell types, as well as between localization mechanisms. For example, localization from the cytoplasm to the nucleus is restricted by the size of the nuclear pore,[2,13] whereas the localization of pro-apoptotic proteins from the cytoplasm to the mitochondria is limited only by the size of the target location. This experiment shows that a relatively small change in the environmental morphology can impact the performance of the localization system. This may explain why certain localization processes that depend on movement through small areas (such as nuclear import) rely on high affinity transport proteins (importins and exportins) whereas localizations to the mitochondria or plasma membrane do not have similar transport mechanisms.

Materials and Methods

Monte Carlo biomolecular simulator

A stochastic simulator was developed for this study based on previous stochastic simulators.[22,24,25,31–38] The simulator tracks the location of each molecule created and allows it to perform a random walk (diffuse) through space in discrete time. Collisions between molecules are the basis of mass action reactions. Complex reactions are modeled as a set of association between two molecules with a set rate, k_f, or dissociation of one molecule into others with a set rate, k_r. The simulation was carried out in a μm scale-down of the *in vitro* experiments.

The specific reactions and reaction rates used are listed in Table I. The diffusion coefficient for all species was 10^{-10} m^2 s^{-1}, however, the proteins bound to beads (CaM and CSH3) were confined to a 0.1 μm depth at the bottom of their respective wells to mimic the thickness of the beads in the *in vitro* implementation (see below). The mass and size (diameter) of all protein components was approximated as 10 kDa and 3 nm, respectively.

Cassette-based fusion proteins and localization system components

All fusion proteins were made using the method of Truong *et al.*[42] The *in vitro* localization sensor was based on a YFP Venus (Ven)[20] fused with two binding peptides at the C terminus. The most C terminal

peptide is one of a Ca^{2+}-dependent CBP, either CKKp or CaMK4p. CKKp has a smaller K_D for CaM than CaMK4p.[18,19] Thus, there are two sensor variants with different kinetics to investigate the affect of kinetics on the system's behavior. The second binding peptide in the sensor is CB1, placed between the CBP and Ven. CSH3 has a micromolar affinity for CB1 as has been reported previously.[21]

Binding domains for the sensor peptides were immobilized using commercial beads assays. CaM resin was used according to manufacturer's directions (Stratagene, La Jolla, CA). A second bead system was used where glutathione (GSH) is covalently bound to a bead and binds glutathione-*s*-transferase (GST) on fusion proteins (Novagen, San Diego, CA). CB1 binding to GSH beads is mediated by an intermediate fusion protein: CSH3-mRFP-GST, where mRFP is a monomeric red fluorescent protein.[40] For simplicity, this type of bead will be referred to as CSH3 beads.

Two-well fluorescent localization constructs

The two-well construct was created with three polyethylene rectangular prisms cut from UVette cuvettes (Eppendorf, Hamburg, Germany). The prisms were arranged on a glass microscope slide such that two prisms were vertically contacting the slide and the third formed a horizontal bridge with the vertical prisms. The region of the two vertical prisms below the bridge connection formed a well. Windows were cut from the facing sides of the vertical prisms to form a continuum with the bridge. All contacting edges were sealed with epoxy resin, whose autofluorescence was controlled with an opaque polyethylene sheet.

For *in vitro* experiments in the two-well constructs, a 1 mm thick layer of beads (100 μL) was prepared according to manufacturer's instructions and carefully laid down in each respective well. Sensor proteins were added to the bridge region so as to not bias the initial localization. The sensors were expressed in *Escherichia Coli* and mechanically extracted: concentration was ~40 μ*M* in a 50 m*M* Tris, 100 m*M* NaCl buffer. This same buffer was used to fill the remainder of the two-well construct. For *in vitro* experiments, unless otherwise noted, the solution was brought to 1 m*M* EDTA in the diffusion phase, then 2 m*M* $CaCl_2$ in the Ca^{2+}-translocation phase, then 4 m*M* EDTA in the EDTA-translocation phase.

Image analysis

Fluorescent localizations were viewed using the Illumatool Tunable Lighting System (Light Tools Research, Encinitas, CA) with 488 nm excitation and 520 nm emission filters for Ven. Photographs were taken using a Canon A350 Powershot camera stored in JPEG format. Analysis was conducted using IrfanView.

Brightness in two regions of an image was compared by forming a localization ratio between them. To accomplish this, the brightness of every pixel in a region of interest was binned from 1 to 256 and the peak of the histogram was selected as the brightness of that region. Then, a ratio was formed as the brightness of region A divided by the brightness of region B. Ratios greater than 1 suggest more protein in region A, less than 1 suggest more protein in region B, while a ratio of 1 suggests no preferential association.

Acknowledgments

This work was supported by a fellowship to E.M. from Natural Science and Engineering Research Council (NSERC) and grants to K.T. from the Canadian Foundation of Innovation, Canadian Institutes of Health Research, Heart and Stroke Foundation, and the Natural Science and Engineering Research Council. E.M. carried out the simulations, experiments, data analysis, and drafted the manuscript. K.T. conceived the study, provided direction, and helped draft the manuscript.

References

1. Johnson AE, van Waes MA (1999) The translocon: a dynamic gateway at the ER membrane. Annu Rev Cell Dev Biol 15:799–842.
2. Sorokin AV, Kim ER, Ovchinnikov LP (2007) Nucleocytoplasmic transport of proteins. Biochemistry (Mosc) 72: 1439–1457.
3. Pertz O, Hodgson L, Klemke RL, Hahn KM (2006) Spatiotemporal dynamics of RhoA activity in migrating cells. Nature 440:1069–1072.
4. Ridley AJ (2006) Rho GTPases and actin dynamics in membrane protrusions and vesicle trafficking. Trends Cell Biol 16:522–529.
5. Haller C, Kiessling F, Kubler W (1998) Polarized expression of heterologous membrane proteins transfected in a human endothelial-derived cell line. Eur J Cell Biol 75: 353–361.
6. Bethune J, Wieland F, Moelleken J (2006) COPI-mediated transport. J Membr Biol 211:65–79.
7. Stommel JM, Marchenko ND, Jimenez GS, Moll UM, Hope TJ, Wahl GM (1999) A leucine-rich nuclear export signal in the p53 tetramerization domain: regulation of subcellular localization and p53 activity by NES masking. EMBO J 18:1660–1672.
8. Mahalakshmi RN, Nagashima K, Ng MY, Inagaki N, Hunziker W, Beguin P (2007) Nuclear transport of Kir/Gem requires specific signals and importin alpha5 and is regulated by calmodulin and predicted serine phosphorylations. Traffic 8:1150–1163.
9. Sim H, Rimmer K, Kelly S, Ludbrook LM, Clayton AH, Harley VR (2005) Defective calmodulin-mediated nuclear transport of the sex-determining region of the Y chromosome (SRY) in XY sex reversal. Mol Endocrinol 19: 1884–1892.
10. Puthalakath H, Strasser A (2002) Keeping killers on a tight leash: transcriptional and post-translational control of the pro-apoptotic activity of BH3-only proteins. Cell Death Differ 9:505–512.
11. Suzuki K, Kostin S, Person V, Elsasser A, Schaper J (2001) Time course of the apoptotic cascade and effects of caspase inhibitors in adult rat ventricular cardiomyocytes. J Mol Cell Cardiol 33:983–994.
12. Mutarelli M, Cicatiello L, Ferraro L, Grober OM, Ravo M, Facchiano AM, Angelini C, Weisz A (2008) Time-course analysis of genome-wide gene expression data from

hormone-responsive human breast cancer cells. BMC Bioinformatics 9 (Suppl 2):S12.
13. Chook YM, Blobel G (2001) Karyopherins and nuclear import. Curr Opin Struct Biol 11:703–715.
14. Lacayo CI, Pincus Z, VanDuijn MM, Wilson CA, Fletcher DA, Gertler FB, Mogilner A, Theriot JA (2007) Emergence of large-scale cell morphology and movement from local actin filament growth dynamics. PLoS Biol 5:e233.
15. Terasawa K, Taguchi T, Momota R, Naito I, Murakami T, Ohtsuka A (2006) Human erythrocytes possess a cytoplasmic endoskeleton containing beta-actin and neurofilament protein. Arch Histol Cytol 69:329–340.
16. Pham E, Li I, Truong K (2008) Computational modeling approaches for studying of synthetic biological networks. Curr Bioinformatics 3:130–141.
17. Crivici A, Ikura M (1995) Molecular and structural basis of target recognition by calmodulin. Ann Rev Biophys Biomol Struct 24:85–116.
18. Marlow MS, Wand AJ (2006) Conformational dynamics of calmodulin in complex with the calmodulin-dependent kinase kinase alpha calmodulin-binding domain. Biochemistry 45:8732–8741.
19. Cruzalegui FH, Means AR (1993) Biochemical-characterization of the multifunctional Ca^{2+}/calmodulin-dependent protein-kinase type-IV expressed in insect cells. J Biol Chem 268:26171–26178.
20. Nagai T, Ibata K, Park ES, Kubota M, Mikoshiba K, Miyawaki A (2002) A variant of yellow fluorescent protein with fast and efficient maturation for cell-biological applications. Nat Biotechnol 20:87–90.
21. Knudsen BS, Zheng J, Feller SM, Mayer JP, Burrell SK, Cowburn D, Hanafusa H (1995) Affinity and specificity requirements for the first Src homology-3 Domain of the Crk proteins. EMBO J 14:2191–2198.
22. Boulianne L, Al Assaad S, Dumontier M, Gross WJ (2008) GridCell: a stochastic particle-based biological system simulator. BMC Syst Biol 2:66.
23. Haseltine EL, Arnold FH (2007) Synthetic gene circuits: design with directed evolution. Annu Rev Biophys Biomol Struct 36:1–19.
24. Adalsteinsson D, McMillen D, Elston TC (2004) Biochemical network stochastic simulator (BioNetS): software for stochastic modeling of biochemical networks. BMC Bioinformatics 5:24.
25. Meng TC, Somani S, Dhar P (2004) Modeling and simulation of biological systems with stochasticity. In Silico Biol 4:293–309.
26. Marguet P, Balagadde F, Tan C, You L (2007) Biology by design: reduction and synthesis of cellular components and behaviour. J R Soc Interface 4:607–623.
27. Newton AC (1997) Regulation of protein kinase C. Curr Opin Cell Biol 9:161–167.
28. Beck M, Forster F, Ecke M, Plitzko JM, Melchior F, Gerisch G, Baumeister W, Medalia O (2004) Nuclear pore complex structure and dynamics revealed by cryoelectron tomography. Science 306:1387–1390.
29. Rakowska A, Danker T, Schneider SW, Oberleithner H (1998) ATP-Induced shape change of nuclear pores visualized with the atomic force microscope. J Membr Biol 163:129–136.
30. Arikawa M, Saito A, Omura G, Mostafa Kamal Khan SM, Suetomo Y, Kakuta S, Suzaki T (2005) Ca^{2+}-dependent nuclear contraction in the heliozoon Actinophrys sol. Cell Calcium 38:447–455.
31. Le Novere N, Shimizu TS (2001) STOCHSIM: modelling of stochastic biomolecular processes. Bioinformatics 17: 575–576.
32. Lok L, Brent R (2005) Automatic generation of cellular reaction networks with moleculizer 1.0. Nat Biotechnol 23:131–136.
33. Mao L, Resat H (2004) Probabilistic representation of gene regulatory networks. Bioinformatics 20:2258–2269.
34. Sanford C, Yip ML, White C, Parkinson J (2006) Cell++--simulating biochemical pathways. Bioinformatics 22:2918–2925.
35. Ohki N, Hagiwara M (2005) Bio-object, a stochastic simulator for post-transcriptional regulation. Bioinformatics 21:2478–2487.
36. Hoops S, Sahle S, Gauges R, Lee C, Pahle J, Simus N, Singhal M, Xu L, Mendes P, Kummer U (2006) COPASI—a complex pathway simulator. Bioinformatics 22:3067–3074.
37. You L, Hoonlor A, Yin J (2003) Modeling biological systems using Dynetica—a simulator of dynamic networks. Bioinformatics 19:435–436.
38. Sedwards S, Mazza T (2007) Cyto-Sim: a formal language model and stochastic simulator of membrane-enclosed biochemical processes. Bioinformatics 23:2800–2802.
39. Tsien R, Pozzan T (1989) Measurement of cytosolic free Ca^{2+} with quin2. Methods Enzymol 172:230–262.
40. Campbell RE, Tour O, Palmer AE, Steinbach PA, Baird GS, Zacharias DA, Tsien RY (2002) A monomeric red fluorescent protein. Proc Natl Acad Sci USA 99:7877–7882.
41. Wen W, Meinkoth JL, Tsien RY, Taylor SS (1995) Identification of a signal for rapid export of proteins from the nucleus. Cell 82:463–473.
42. Truong K, Khorchid A, Ikura M (2003) A fluorescent cassette-based strategy for engineering multiple domain fusion proteins. BMC Biotechnol 3:8.